The bulk parameterizations of turbulent air-sea fluxes in NEMO4: the origin of Sea Surface Temperature differences in a global model study

Giulia Bonino[1*], Doroteaciro Iovino[1], Laurent Brodeau[2], and Simona Masina[1]

[1]Ocean Modeling and Data Assimilation Division, Centro Euro-Mediterraneo sui Cambiamenti Climatici, Bologna, Italy.
[2]Centre National de la Recherche Scientifique, IGE/MEOM, Grenoble, France

Correspondence: Giulia Bonino (giulia.bonino@cmcc.it)

Abstract.

Wind stress and turbulent heat fluxes are the major driving forces that modify the ocean dynamics and thermodynamics. In the Nucleus for European Modelling of the Ocean (NEMO) ocean general circulation model, these turbulent air-sea fluxes (TASFs) can critically impact the simulated ocean characteristics. This paper investigates how the various bulk parameterizations to calculate turbulent air-sea fluxes in NEMOv4 can lead to substantial differences in the estimation of sea surface temperatures (SST). Specifically, we study the contribution of different aspects and assumptions of the bulk parameterizations in driving the SST differences in NEMO global model configuration at ¼ degree of horizontal resolution. These aspects include the use of the skin temperature instead of the bulk SST in the computation of turbulent heat flux components and the estimation of wind stress and of turbulent heat flux components, which vary in each parameterization due to different bulk transfer coefficients. The analysis of a set of short-term sensitivity experiments, where the only change is related to one of the aspects of the bulk parameterizations, shows that parameterization-related SST differences are primarily sensitive to wind stress differences and to the implementation of skin temperature in the computation of turbulent heat flux components. In addition, in order to highlight the role of SST-turbulent heat flux negative feedback at play in ocean simulations, we compare the TASF differences obtained using the NEMO ocean model with the estimations by Brodeau et al. (2017), who compared the different bulk parameterizations using prescribed SST. Our estimations of turbulent heat flux differences between bulk parameterizations are weaker than those found by Brodeau et al. (2017).

1 Introduction

Ocean and atmosphere circulations are highly influenced by the transfer of momentum and heat at the air-sea interface (e.g., Gill, 1982; Siedler et al., 2013). These transfers of energy are primarily driven by surface radiative flux and turbulent air-sea fluxes (TASFs), which include wind stress and turbulent heat flux components (THFs, latent and sensible heat fluxes). In the upper ocean, wind stress is a major driving force of basin-scale circulation (e.g., Chen et al., 1994; Shriver and Hurlburt, 1997), and THFs are important for determining its thermal properties (e.g., Yuen et al., 1992; Swenson and Hansen, 1999). Therefore,

both wind stress and THFs are important for the evolution of sea surface temperature (SST), because of their contribution to turbulent mixing within the ocean surface mixed layer (e.g., Barnier, 1998).

Since direct observations of TASFs are sparse in space and time, the estimates are derived using bulk formulas, which relate each component of turbulent air-sea flux to more easily measurable and widely available meteorological surface atmospheric variables (e.g. wind speed, air temperature, air specific humidity) through bulk transfer coefficients. These coefficients are estimated using bulk parameterizations. Different bulk parameterizations are currently used which are traditionally developed statistically, comparing in situ meteorological observations of surface atmospheric variables with TASFs derived from ship and buoy measurements (Large and Pond, 1981, 1982; Smith, 1988; Fairall et al., 1996, 2003; Bradley and Fairall, 2007; Edson et al., 2013).

In the NEMO ocean general circulation model (OGCM), TASFs are computed by means of bulk formulas using prescribed surface atmospheric variables (air temperature, air humidity, wind) and the prognostic SST of the model (hereinafter online prognostic SST approach). This approach incorporates the response of the ocean (i.e. SST) to atmospheric events into the estimation of the THFs and of longwave radiation (i.e. non solar heat flux components, NSHFs) at each time step of the numerical experiment. The feedback between the ocean and the atmosphere partially simulate the energy exchange between them (Kara et al., 2000). The OGCM entails the selecting a given bulk parameterization, which influences the magnitude of the wind stress and the THFs (Kara et al., 2000). The TASFs affect the simulated ocean characteristics and in particular the evolution of the SST (Torres et al., 2019). The online prognostic approach only partially closes the air-sea feedback. Surface winds and clouds are affected by the SST structure on daily time-scales which, in turn, affect the SST and the TASFs (Desbiolles et al., 2021; de Szoeke et al., 2021; Gaube et al., 2019; Li and Carbone, 2012; Small et al., 2008). The closed air-sea feedback (hereinafter coupled approach) in the system could substantially impact the turbulent fluxes (Lemarié et al., 2021; Small et al., 2008), however the coupled approach is still not yet mature in the ocean model community. Recently Lemarié et al. (2021) exploited a simplified atmospheric boundary layer model (ABL) to improve the representation of air-sea interactions in NEMOv4.2. However, the online prognostic SST approach is still widely used by the ocean modeling community in a variety of applications.

Brodeau et al. (2017) compared a set of bulk parameterizations which compute TASFs using prescribed SST (hereinafter offline prescribed SST approach) rather than the prognostic SST of the model. They reported that the use of different bulk parameterizations to estimate TASFs can typically produce differences in total turbulent heat flux (Q_T, i.e. the sum of the THFs, latent and sensible heat fluxes) of about $10W/m^2$ and in wind stress of about $20mN/m^2$. The online prognostic SST approach, used in the NEMO experiments performed in our study, can substantially modify these estimates through the negative SST feedback on Q_T, which likely dampens the Q_T discrepancies across the various bulk parameterizations (Seager et al., 1995).

The aim of this work is to better understand the response of the prognostic SST to the TASFs and to their parameterization in NEMO version 4.0 at 1/4° of horizontal resolution. We also discuss the role of the SST-Q_T negative feedback at play in the online prognostic SST approach. We address the sensitivity of the SST to various aspects of the different bulk parameterizations, such as the inclusion of the skin temperature in the computation of the THFs and the role of bulk transfer coefficients in the

estimation of the wind stress and THFs. We thus analysed differences between short-term sensitivity experiments where bulk assumptions are excluded (e.g. skin temperature) or where bulk transfer coefficients are computed mixing the different bulk parameterizations. Lastly, in order to highlight the role of the SST-Q_T negative feedback at play in our online prognostic SST approach, we compare TASFs with the estimations from Brodeau et al. (2017). We also provide a simple validation of the various experiments against an SST observed dataset, however the main objective of the work was to investigate the impact of a set of bulk parameterizations on the SST generated by NEMO rather than evaluating their accuracy in reproducing it.

This paper is organized as follows. Section 2 presents the model used for this study, a short overview of the bulk formulas implemented in NEMOv4, the experimental set-up and the modifications introduced in the bulk parameterizations used for the sensitivity experiments. In Section 3 we present the parameterization-related SST discrepancies, quantify SST discrepancies related to various aspects of the different bulk parameterizations and compare and discuss our findings with the literature. Our conclusions are drawn in Section 4.

2 Model configuration, bulk forcing and experimental set-up

2.1 NEMOv4 model configuration

The sensitivity of prognostic SST to bulk parameterizations is investigated in a numerical study using the Nucleus for European Modelling of the Ocean[1] (NEMO, version 4.0, revision 12957). NEMO is a three-dimensional, free-surface, hydrostatic, primitive-equation global ocean general circulation model (Madec G. and NEMO System Team,) coupled to the Sea Ice modelling Integrated Initiative (SI^3, NEMO Sea Ice Working Group, 2020). Our configuration uses the global ORCA025 tripolar grid (Madec and Imbard, 1996) with 1/4° horizontal resolution (27.75km) at the Equator, which increases with latitudes, e.g. 14km at 60 °. The vertical grid has 75 levels, whose spacing increases with a double hyperbolic tangent function of depth from 1 m near the surface to 200 m at the bottom, with partial steps representing the topography of the bottom (Bernard et al., 2006). The bathymetry of the model is based on the combination of the ETOPO1 data set (Amante and Eakins, 2009) in the open ocean and GEBCO (IOC, 2003) in coastal regions. The horizontal turbulent viscosity is parameterized by means of a biharmonic function with a value of $1.8 \times 10^{11} m^4 s^{-1}$ at the Equator, reducing poleward as the cube of the maximum grid cell size. The advection of the tracers uses a total variance dissipation (TVD) scheme (Zalesak, 1979). The Laplacian lateral tracer mixing is along isoneutral surfaces with a coefficient of $300 m^2 s^{-1}$. The vertical mixing of tracers and momentum is parameterised using the turbulent kinetic energy (TKE) scheme (Blanke and Delecluse, 1993). Subgrid-scale vertical mixing processes are represented by a background vertical eddy diffusivity of $1.2 \times 10^{-5} m^2 s^{-1}$ and a globally constant background viscosity of $1.2 \times 10^{-4} m^2 s^{-1}$. The friction at the bottom is quadratic, and a diffusive bottom boundary layer scheme is included. The continental runoff data are a monthly climatology derived from the global river flow and continental discharge dataset for the major rivers (Dai and Trenberth, 2002; Dai et al., 2009), and estimates by Jacobs et al. (1996) for the Antarctic coastal freshwater discharge. The initial conditions for temperature and salinity are provided by the World Ocean Atlas 2013

[1] https://www.nemo-ocean.eu/

(Levitus et al., 2013). All the experiments are forced with the hourly ERA5 Reanalysis of the ECWMWF (Hersbach et al., 2020).

2.2 The bulk formulas and their parameterization in NEMO4.0

As stated in the introduction, NEMO uses the online prognostic SST approach to compute TASFs, which are estimated using the prognostic SST and prescribed atmospheric surface variables by means of aerodynamic bulk formulas:

$$\tau = \rho C_D U \mathbf{u_z} \tag{1a}$$

$$Q_H = \rho C_p C_H (\theta_z - T_s) U \tag{1b}$$

$$E = \rho C_E (q_0 - q_z) U \tag{1c}$$

$$Q_L = -L_v E \tag{1d}$$

where τ is the wind stress, Q_H is the turbulent flux of sensible heat, E is the evaporation, and Q_L is the turbulent flux of latent heat. Throughout this paper, we use the convention that a positive sign of τ, of THFs (Q_H and Q_L), and of the total turbulent heat flux Q_T ($Q_T = Q_H + Q_L$) means a gain in the relevant quantity for the ocean. The term ρ is the density of air; C_p is the heat capacity of moist air, and L_v is the latent heat of vaporization. $\mathbf{u_z}$ is the wind speed vector at height z, which may be absolute or relative to the ocean currents. The bulk scalar wind speed U is the scalar wind speed $|\mathbf{u_z}|$ with the potential inclusion gustiness. Convective gustiness is a temporary increase in the wind speed due to the friction and the free convection, and is active and significant in very calm wind conditions with an unstable near-surface atmosphere. It is added to the wind speed and avoids zero wind singularity. θ_z and q_z are the potential temperature and specific humidity of air at height z, while T_s, q_0 are the potential temperature and specific humidity at the surface. Depending on the bulk parameterization used, T_s can be the temperature at the air-sea interface (sea surface skin temperature, SSTskin) or typically at a depth of one meter (bulk sea surface temperature, SST). The SSTskin differs from the SST due to two effects with opposite signs: the cool skin and warm layer (CSWL). The cool skin is the cooling of the millimeter-scale uppermost layer of the ocean, which ensures a steep vertical gradient of temperature that sustains the heat flux continuity between the ocean and atmosphere. The warm layer is the warming of the upper few meters of the ocean in daytime and sunny conditions.

C_D, C_H, and C_E are the Bulk Transfer Coefficients (BTCs) for wind stress, sensible heat, and moisture, respectively.

The main differences between bulk parameterizations are therefore usually related to:

1. The use of the skin temperature (hereinafter SSTskin) rather than the bulk SST in the estimation of near surface atmospheric stability and bulk formulas.

2. The dependence of the exchange coefficients on the wind speed

3. The inclusion of convective gustiness in the wind calculation

4. The effect of including ocean currents in wind stress

In this study, we disentangle the effects of the first two aspects on SST (Sections 3.2, 3.3 and 3.4), and discuss the effect of the inclusion of convective gustiness in the wind stress computation (Section 3.4). The effects of the ocean current interaction/feedback in the bulk formulation has been widely explored (e.g. Renault et al., 2019a, b; Sun et al., 2019). Although many studies have highlighted the substantial difference in the surface input to the ocean between calculations that use absolute vs. relative wind, we decided to leave this aspect to future work since the implementation of this correction essentially depends on the characteristics of the forcing fields (Renault et al., 2020).

The online prognostic SST approach of NEMO uses the modelled SST at each time step to estimate NSHFs (i.e. THFs + long wave radiation). In our experiments, we only focus on the NSHFs computed by bulk formulas, namely the THFs. The SST responds to the total turbulent heat flux Q_T at each time step: the Q_T generate SST anomalies, and SST anomalies, in turn, modulate Q_T. Specifically, SST and Q_T feedback negatively: when the SST becomes anomalously cold, then Q_T increases, which increases SST, then QT will decrease, and so on. This negative feedback of the online prognostic SST reduces the differences in heat fluxes across the different bulk parameterizations. On the other hand, the wind stress is not affected by this type of first-order feedback at play for the Q_T.

In this study we focus on three bulk parameterizations implemented in NEMOv4: NCAR (Large and Yeager, 2009), COARE 3.6 (Edson et al. (2013) + Chris Fairall, private communication, hereinafter referred to as "COARE"), and ECMWF as coded in the Aereobulk package (Brodeau et al., 2017). All the codes to estimate TASFs in the NEMOv4.0 framework, originate from this AeroBulk package (Brodeau et al., 2017).

COARE and ECMWF parameterizations are designed to be used with the SSTskin, so that the two algorithms include a CSWL parameterization to estimate it. NCAR uses the bulk SST in the heat flux calculation and the zero-wind singularity is avoided by simply setting a minimum value for the scalar wind speed at $0.5m/s$. To calculate the BTCs, the bulk parameterizations rely on an empirical closure. More specifically, in COARE and ECMWF parameterizations, the computation of BTCs uses the Monin-Obukhov similarity theory (MOST, Monin and Obukhov, 1954). As such, BTCs are a function of the roughness lengths and of the stability of the atmospheric surface layer. The NCAR parameterization uses a combination of the MOST theory with a semi-empirical form of the drag coefficient in which the BTCs are computed as a function of neutral wind speed (e.g. the wind speed in neutral stability conditions and at 10m reference level, U_{N10}). The BTCs are shifted to the current atmospheric stability. Figure 1 shows the U_{N10} annual mean and the neutral BTCs as a function of U_{N10} for the selected bulk formula parameterizations. Due to the stronger neutral drag coefficient C_D^{N10}, the NCAR parameterization tends to enhance wind stress with respect to COARE and to ECMWF under light wind conditions ($u < 5m/s$). On the other hand,

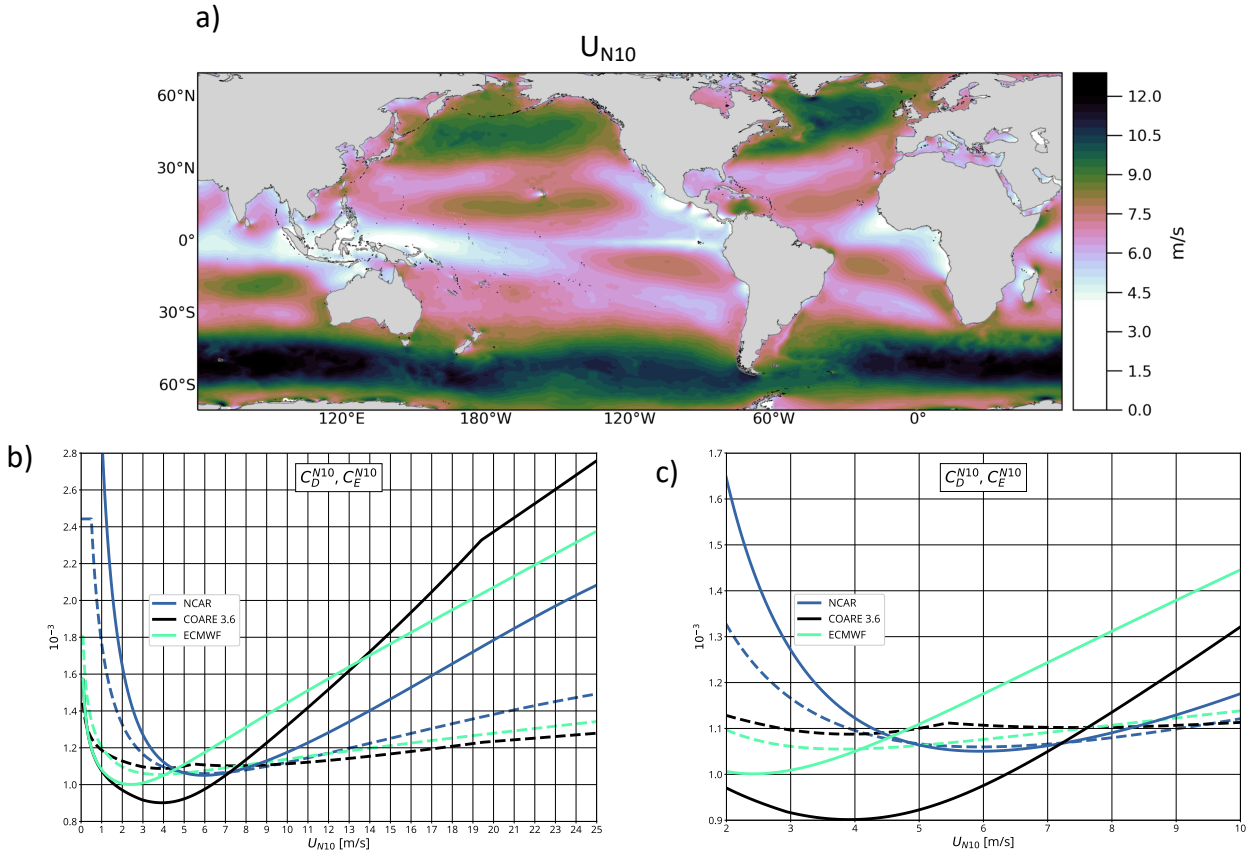

Figure 1. a) Annual mean U_{N10} from NCAR parameterization b) Neutral drag and moisture transfer coefficients (C_D^{N10} and C_E^{N10}) for COARE (black), NCAR (blue), and ECMWF (green) bulk parameterizations (solid and dashed lines, respectively), as functions of the neutral wind speed at 10 m; c) zoom of panel b) for the wind range $2 - 10m/s$

the ECMWF parameterization enhances wind stress with respect to NCAR and COARE for wind speeds above $5m/s$, while COARE enhances it for wind speeds above $13m/s$. Under weak-wind conditions, the NCAR parameterization tends to enhance evaporation with respect to COARE and ECMWF due to the stronger C_E^{N10} (see Figure 1). For a detailed explanation of the BTC derivation for each bulk parameterization, please refer to the technical report by Bonino et al. (2020).

2.3 Experimental set-up

In order to investigate the role of different aspects of bulk parameterizations in driving prognostic SST, we performed six numerical experiments (Table 1). All the experiments lasted one year, starting from January 2016 after a one-year spin-up. There is no intent to analyze this year in relation to a specific climatic mode. The simulations are forced by the hourly surface atmospheric variables of the ERA5 Reanalysis (Hersbach et al., 2020).

We first performed three experiments (hereinafter 'control experiments') in order to quantify the bulk parameterization-related SST discrepancies. In particular, we performed ECMWF_S, COARE_S and NCAR experiments, which use the ECMWF, COARE and NCAR parameterizations, respectively. ECMWF_S and COARE_S experiments use the SSTskin (through their respective CSWL scheme) and consider convective gustiness in the wind speed calculation. In contrast, the NCAR experiment computes THFs using bulk SST and the convective gustiness is not considered in the wind speed computation.

In order to disentangle the contribution of the skin temperature and the contribution of the different wind stress and THFs in driving sea surface temperature differences, we performed three sensitivity experiments (hereinafter 'mixed experiments'). First, we performed the ECMWF_NS experiment, which uses the ECMWF parameterization, and THFs are computed using bulk SST rather than SSTskin. Second, we performed the CdNC_CeEC_NS experiment, which uses the ECMWF parameterization to calculate C_H and C_E BTCs and the NCAR bulk formula to calculate C_D BTC. THFs are computed using bulk SST. We also performed an additional experiment, called ECMWF_NS_NG, which differs from ECMWF_NS only in terms of the exclusion of the convective gustiness in the wind speed calculation. We used the absolute wind, which means that the parameterizations do not include the ocean current feedback to calculate the wind in equation 1a.

Experiment name	sea surface temperature used (T_s)	computation of C_D	computation of C_E and C_H	convective gustiness
COARE_S	SSTskin	COARE3.6	COARE3.6	Yes
ECMWF_S	SSTskin	ECMWF	ECMWF	Yes
NCAR	SST	NCAR	NCAR	No
ECMWF_NS	SST	ECMWF	ECMWF	Yes
CdNC_CeEC_NS	SST	NCAR	ECMWF	No
ECMWF_NS_NG	SST	ECMWF	ECMWF	No

Table 1. Summary of the numerical experiments.

3 Results

Here we discuss the parameterization-related discrepancies in the control experiments in terms of TASFs (i.e. Q_T and τ), WSC, SST and meridional heat transport (section 3.1). Then, we try to analyze the contribution of various aspects of the parame-

terizations in driving these SST and meridional transport discrepancies. In particular, the comparison between ECMWF_S and ECMWF_NS is used to determine the skin temperature contribution (section 3.2), while the comparisons between CdNC_CeEC_NS and NCAR (section 3.3) and between CdNC_CeEC_NS and ECMWF_NS (section 3.4) teach us about the Bulk Transfer Coefficients contribution. In section 3.4, we also compare ECMWF_NS_NG and ECMWF_NS experiments to show the effect of the inclusion of convective gustiness in the wind speed calculation on wind stress computation (shown in the supplementary material). For each pair of experiments, we only show the differences in TASFs and their components (e.g. U,C_D, C_E) which are relevant to understand the SST or meridional heat transport discrepancies. The complementary TASFs differences are reported in the supplementary material. We analyze annual mean differences between experiments and assess their statistical significance using t-test.

3.1 Parameterization-related discrepancies

We compared the SST simulated by the ECMWF_S, COARE_S and NCAR control experiments with the European Space Agency (ESA) Climate Change Initiative (CCI) SST dataset v2.0 (hereinafter ESA CCI SST dataset) which consists of daily-averaged global maps of SST on a 0.05° x 0.05° regular grid, covering the period from September 1981 to December 2016 (Merchant et al., 2019). All the control experiments present a warm bias in the Eastern Pacific, in the Eastern Boundary Upwelling systems (EBUS), in the Western Boundary Currents (WBCs) and in the Antarctic Circumpolar Current (ACC) region. The SST reproduced by COARE_S and ECMWF_S shows a cold bias of about -1°C in the North Atlantic open ocean at mid-latitudes, and a warm bias of about 0.5°C in the Indian Ocean and the Western Pacific (Figure 2a,b). The NCAR SST is also colder than observations, with a larger bias of about -2°Cin the North Atlantic (Figure 2c). The bias is generally higher compared with the other two experiments and covers wider areas.

Figure 3 shows the differences in total turbulent heat fluxes, wind stress and wind stress curl, from ECMWF_S and COARE_S with respect to NCAR. ECMWF_S wind stress is slightly weaker with respect to NCAR over the equatorial band and is stronger elsewhere (Figure 3a). In COARE_S the wind stress is weaker than NCAR over a broader region with respect to ECMWF_S, namely over the areas characterized by calm wind conditions (see Figure 1). The wind stress curl (WSC) patterns are similar for the two pairs of differences (Figure 3c), and differ only in terms of their magnitude. As regards the Q_T differences (Figure 3b), a gain of heat for ECMWF_S is a clear feature over the Pacific and Atlantic equatorial regions and over EBUS with respect to NCAR.

These TASFs probably cause substantial SST differences between experiments (Figure 4). While the SST in COARE_S is warmer than in NCAR everywhere, overall the SST in ECMWF_S is warmer than in NCAR, but with a colder area (down to -0.6°C) over EBUS and over the Pacific and Atlantic equatorial regions. This spatial pattern of SST differences persists when extending the simulations for up to 5 years (not shown). In these experiments, which differ only in terms of the bulk parameterization, SST differences can arise from the differences in the wind stress and in the THFs as computed by the chosen bulk parameterization (Figure 3). In particular, due to the computation of C_D and the inclusion of the convective gustiness, the wind stress discrepancies may impact on the ocean dynamics by modifying the 3D ocean circulation and mixing and hence the pattern of the SST. The differences in THFs, due to the C_E and C_H computation and the CSWL scheme, may affect the SST

through modifications of the heat loss to the atmosphere . Furthermore, differences in the wind stress and in THFs may also act together by amplifying or damping their individual effects on the SST.

Changes in the simulated SST can reflect on the temperature profile in the upper ocean and the distribution of heat on a global scale. We computed the global ocean heat transport in the upper 100 meters and compared it among our various experiments. Figure 4 (c,d) presents the meridional heat transport (MHT) as a function of latitude. The MHT is larger in ECMWF_S compared to NCAR mostly at all latitudes (Figure 4c), with the largest differences (about 0.8 PW, 20% of NCAR absolute value) in the tropical band where the ECMWF_S wind stress is stronger than NCAR one (Figure 3a). COARE_S and NCAR compare well, with differences lower than 0.3 PW (Figure 4d). We thus focus only on the differences between ECMWF_S andNCAR in order to analyze the relationship between TASFs and SST. We show differences in MHT only when relevant. It is worth mentioning that the annual mean differences (i.e. SST, τ, WSC and Q_T) of each pair of experiments discussed in the following sections sum up linearly to give the annual mean difference between ECMWF_S and NCAR (not shown).

3.2 Skin temperature

The ECMWF and COARE parameterizations, in contrast to NCAR, expect SSTskin as the surface temperature input in order to estimate the near surface atmospheric stability and to compute the THFs. The SSTskin is also used to estimate the upward long wave flux, which is required by the CSWL scheme as a component of the NSHFs. We now compare the results between ECMWF_S and ECMWF_NS to understand the impact of the CSWL implementation in causing the differences in the THFs and thus in the SST shown in Figure 4 (see Table 1 for experiment details). We discuss the impact of the use of skin temperature on the ECMWF parameterization, however similar results are found using COARE (not shown). The ECMWF_S experiment uses the CSWL scheme, so that $T_s \equiv SSTskin$ is used to compute THFs, as opposed to ECMWF_NS in which $T_s \equiv SST$. Consideration of the CSWL effect yields an SST global mean warming of 0.2°C (Figure 5c), with a maximum of 0.3°C over the western equatorial Pacific Ocean, in the Indo-Pacific Warm Pool. In the tropical eastern and Northern Pacific Ocean, and over ACC, the differences are below 0.1°C. the global-mean SSTskin tends to be about 0.1°C colder than the SST (Figure 5a). On a global average basis, the cool skin process predominates over the warm layer effect. Specifically, evaporation occurs almost everywhere and most of the time, while the warm layer builds up only under sunny and low wind conditions.

The colder T_s in ECMWF_S with respect to ECMWF_NS yields a slightly weaker heat loss to the atmosphere due to the decreased NSHFs (mostly evaporation). In ECMWF_S the weaker heat loss to the atmosphere implies a heat gain by the ocean (positive regions in Figure 5b) of approximately $1W/m^2$ on global average compared to ECMWF_NS. We can conclude that the negative SST discrepancies between parameterizations noted in Section 3.1 (Figure 4a) are not explained by the use of the CSWL scheme in the ECMWF parameterization. Nevertheless, the CSWL scheme has a large impact on the positive SST difference between ECMWF_S and NCAR. The SST differences between ECMWF_NS and NCAR (Figure 6a) with respect to the SST differences between ECMWF_S and NCAR (Figure 4) present a reduction in the overall warm temperature differences. τ and WSC differences are shown in Figure S1.

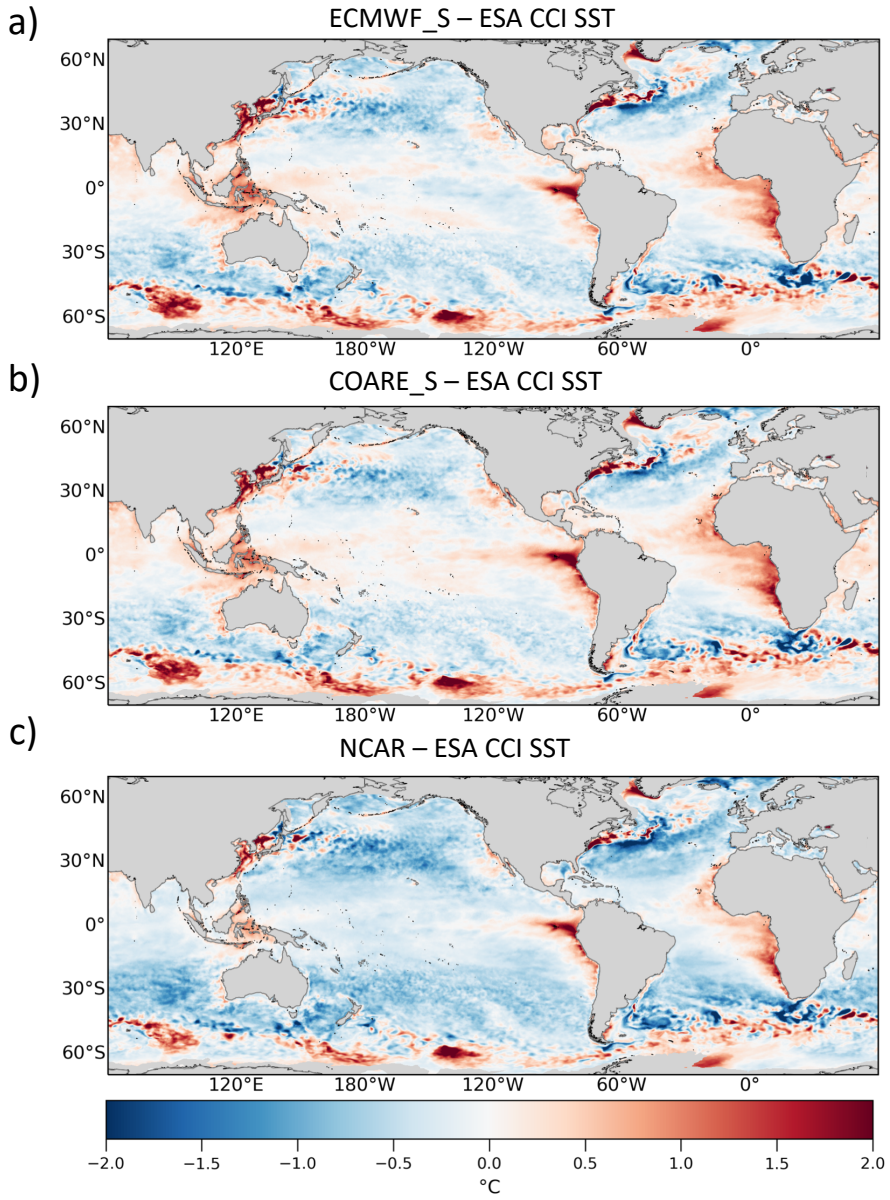

Figure 2. Annual mean SST differences between a) `ECMWF_S` b) `COARE_S`, c) `NCAR` against ESA CCI SST.

3.3 Turbulent Heat fluxes

In order to investigate the effect of the different computations of the THFs between `ECMWF_S` and `NCAR` in driving SST differences (Figure 4a), we compared the results between `CdNC_CeEC_NS` and `NCAR` (see Table 1 for experiments details).

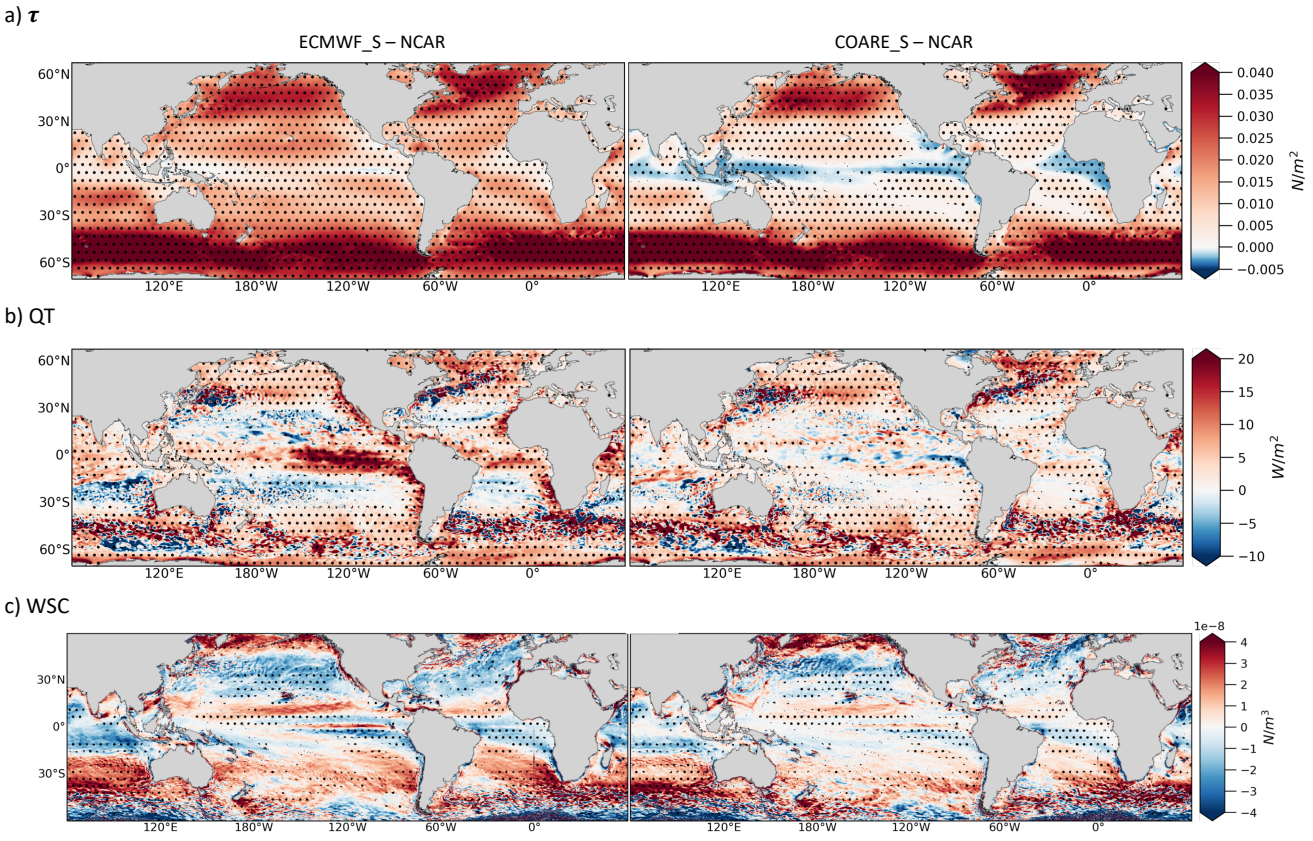

Figure 3. Annual mean differences between experiments on a) wind stress (τ) and b) total turbulent heat fluxes (QT) and c) wind stress curl (WSC) between ECMWF_S and NCAR experiments (left) and COARE_S and NCAR experiments (right). Hatching indicates significant values (95% confidence level)

The SST difference between CdNC_CeEC_NS and NCAR does not show the cold bias over EBUS and over the equatorial Atlantic and Pacific as we found between experiments ECMWF_S and NCAR (compare Figure 4a with Figure 6c). Over those areas, the SST in CdNC_CeEC_NS is warmer than in NCAR of about 0.3°C on average.

As shown in Figure 7a, CdNC_CeEC_NS receives an excess of Q_T of about $1 W/m^2$ on average with respect to NCAR. The main contributor to this difference is the latent heat (Figure 7a and Figure 8b), resulting from the use of a different C_E in the two experiments. The C_E of CdNC_CeEC_NS, which is smaller than C_E of NCAR (Figure 8a), induces weak evaporation. The resulting weaker heat loss to the atmosphere in CdNC_CeEC_NS with respect to NCAR implies a gain of heat by the ocean (positive regions in Figure 7a) of about $2 W/m^2$ over low-latitudes and up to 6 W/m^2 over mid-latitudes (Figure 7b). A similar process also occurs in areas where the annual mean pattern of QT is patchy due to the mesoscale activities in both summer and winter (e.g. in the Western Boundary Currents, Figure S2). In CdNC_CeEC_NS, the negative virtual temperature differences at the air-sea interface are smaller than NCAR, inducing weaker heat losses from the ocean to the atmosphere. It is

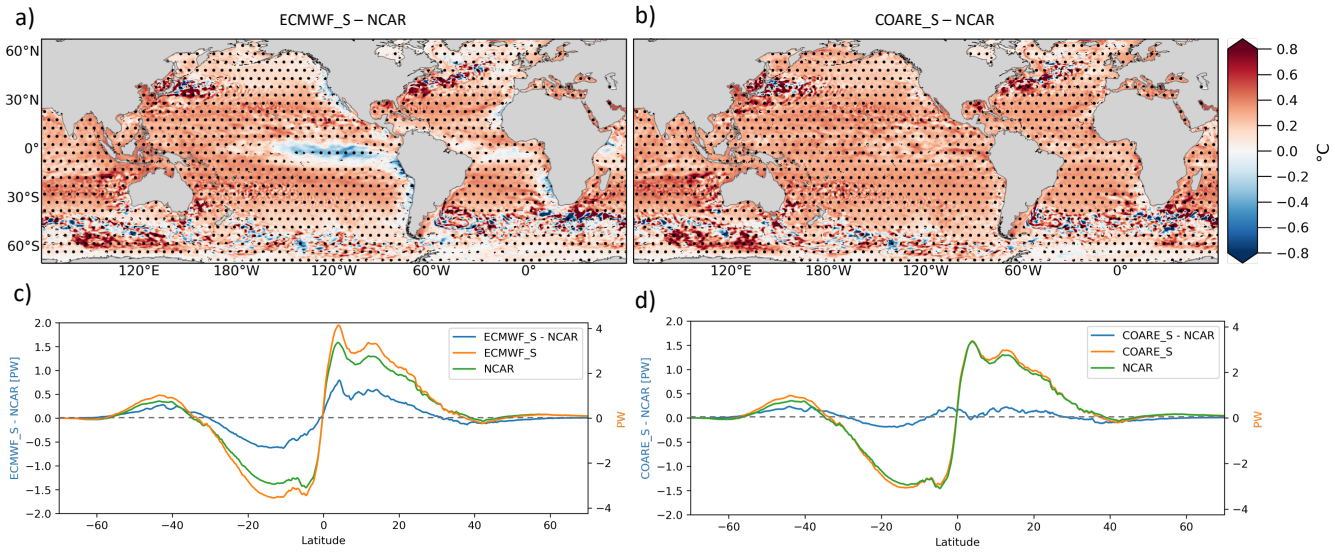

Figure 4. Annual mean SST differences between a) ECMWF_S-NCAR and b) COARE_S - NCAR; Global Meridional Heat Transport values on the right y axis) and differences (values on the left y axis) in the upper 100m ocean between c) ECMWF_S and NCAR and d) COARE_S and NCAR. Hatching indicates significant values (95% confidence level).

worth mentioning that the one-year simulation might not be adequate to properly represent the mean state in WBCs regions due to the chaotic dynamics of these regions - this may explain some of the noise in the difference maps. However, this does not affect the robustness of the results.

The differences in Q_T and SST have the same sign, which suggests that Q_T drives the SST differences. As is clearly shown by the annual zonally-averaged differences (Figure 7b): the weaker the heat loss from the ocean in CdNC_CeEC_NS along the latitude, the warmer the ocean modeled by the CdNC_CeEC_NS experiment with respect to NCAR. τ and WSC differences are shown in Figure S3.

In summary, weak evaporation and thus the weaker heat loss in CdNC_CeEC_NS generates an ocean surface temperature that is warmer than NCAR.

3.4 Drag coefficient and Wind stress

We investigated the impact of the wind stress in driving the SST differences between ECMWF_S and NCAR bulk parameterizations by comparing results from ECMWF_NS and CdNC_CeEC_NS simulations (see Table 1 for experiments details). CdNC_CeEC_NS differs from ECMWF_NS for the use of a different algorithm to compute C_D and for the inclusion of gustiness in the stress computation.

The SST simulated by ECMWF_NS is colder than CdNC_CeEC_NS over EBUS and the tropical Pacific and Atlantic oceans (Figure 6b), which are characterized by wind-driven upwelling. This suggests that wind stress is a major driver of the SST differences (Figure 4a). Referring to Equation 1a, the wind stress is proportional to the wind speed vector at height z ($\mathbf{u_z}$), the

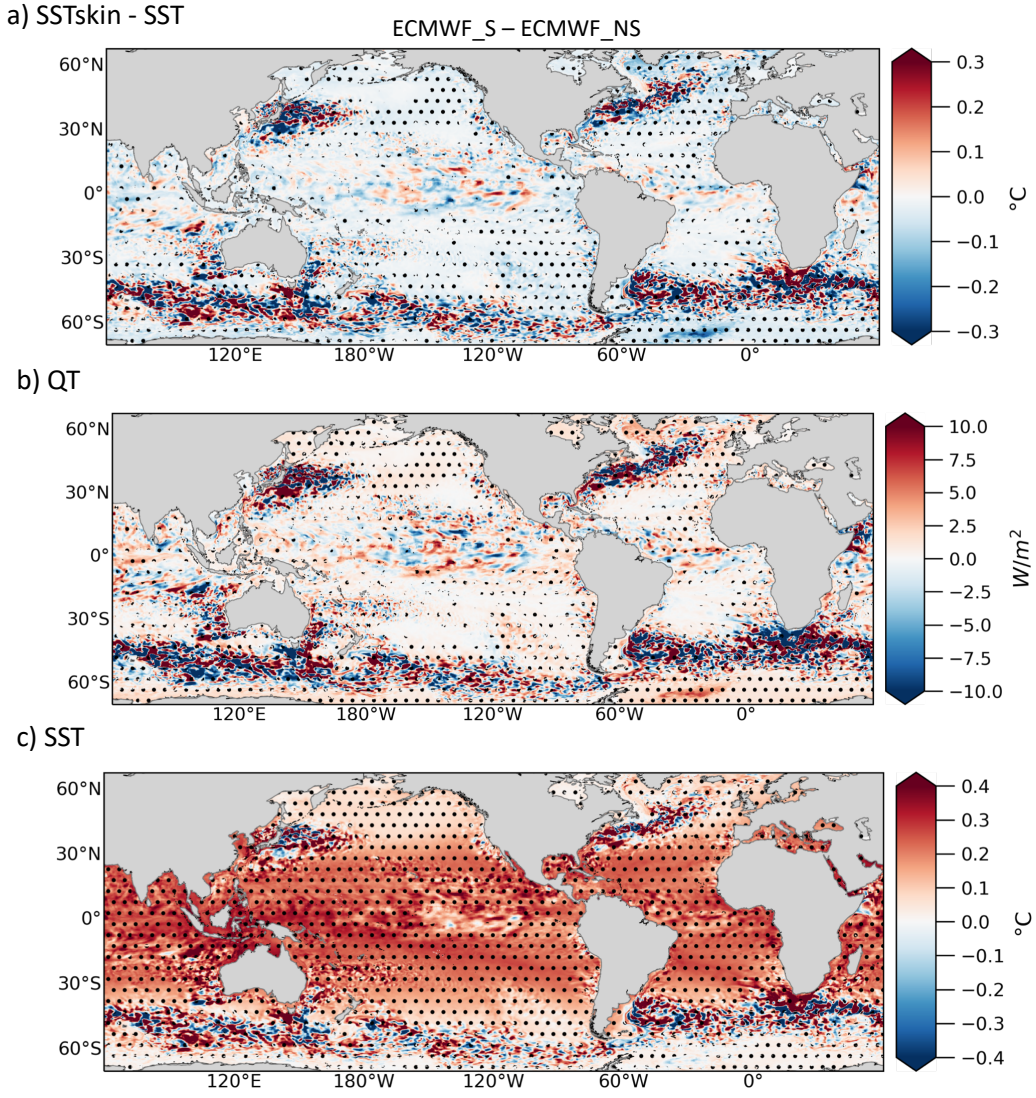

Figure 5. Annual mean differences of a) SSTskin-SST, b) total turbulent heat fluxes (Q_T) and c) SST between ECMWF_S- ECMWF_NS. Hatching indicates significant values (95% confidence level).

bulk scalar wind speed U (with the potential inclusion of a gustiness contribution), and the drag coefficient (C_D). Since U does not depend on SST and on C_D, including gustiness in the ECMWF calculation produces the scalar wind speed differences in Figure 9a. As expected, the differences caused by the gustiness correction, which do not exceed $0.3m/s$, emerge in regions with calm and unstable conditions. These areas are in fact located in the 5°N - 10°N latitude band, in the eastern Pacific and Atlantic oceans, in the tropical western Pacific including the southern China Sea, and the tropical Indian Ocean. Differences in C_D and C_D^{N10} fields between experiments show similar patterns (Figure 9b-c), suggesting that the differences in C_D between

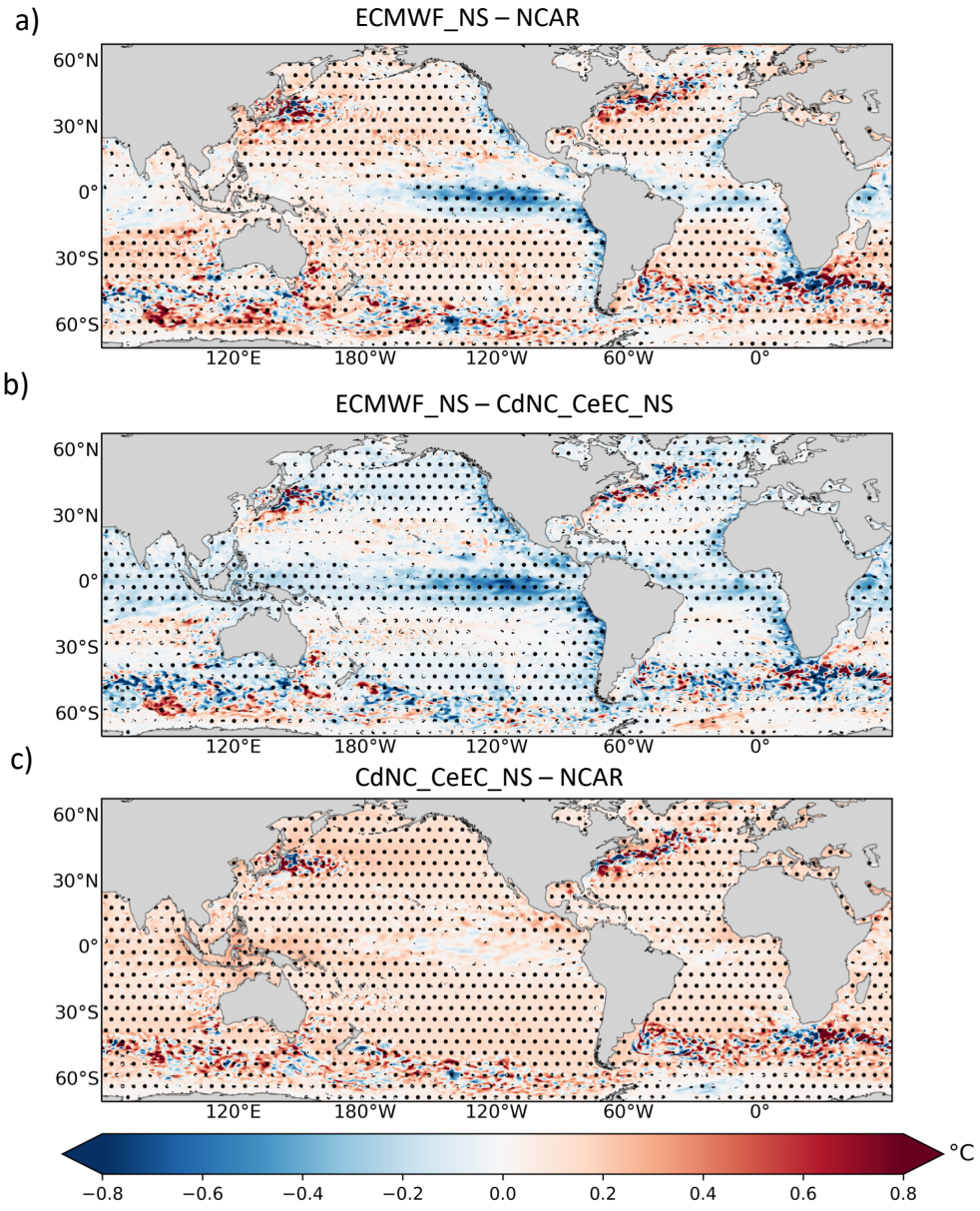

Figure 6. Annual mean SST differences between a) `ECMWF_NS` - `NCAR`, b) `ECMWF_NS` - `CdNC_CeEC_NS`, c) `CdNC_CeEC_NS` - `NCAR`. Hatching indicates significant values (95% confidence level).

parameterizations are related to the neutral coefficient (C_D^{N10}) calculation rather than to its stability correction (term to add to C_D^{N10} to obtain C_D coefficients). In fact, as discussed in Section 2.2 for C_D^{N10}, the ECMWF C_D is larger than NCAR for wind speeds above 5 m/s, and smaller than NCAR for calm up to light breeze conditions (U < 5 m/s). In the areas where U is

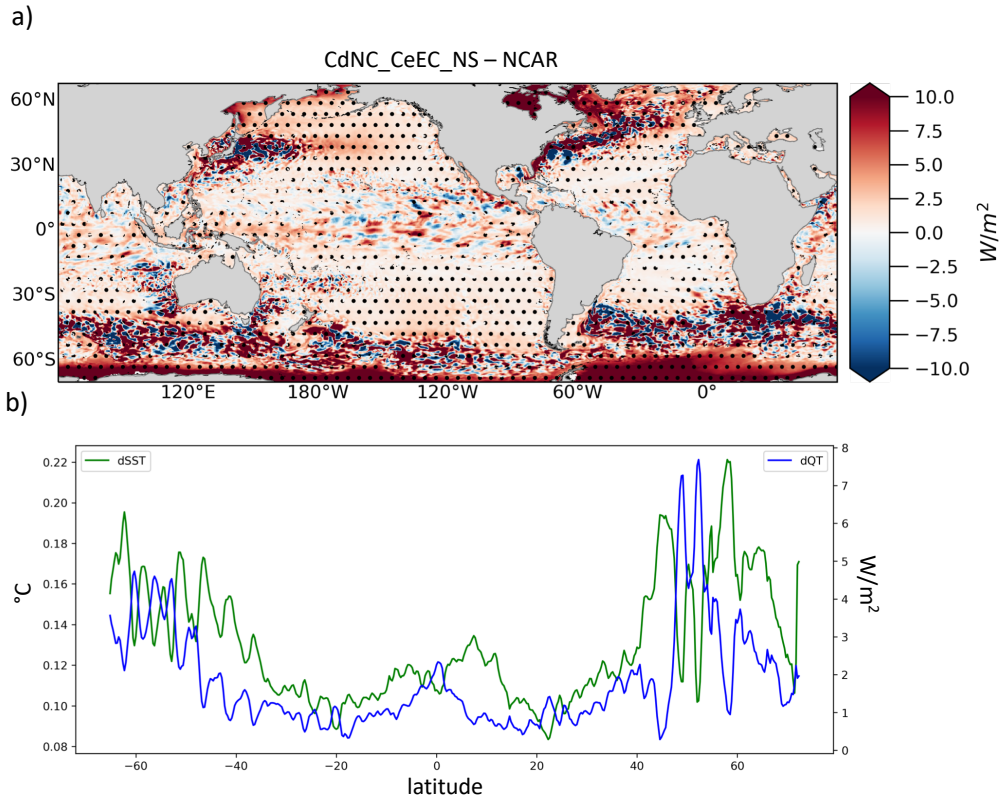

Figure 7. a) Annual mean differences of total turbulent heat fluxes QT between CdNC_CeEC_NS and NCAR experiments. b) zonally-averaged differences in SST (green) and Q_T (blue) annual means between the same experiments. Hatching indicates significant values (95% confidence level).

approximately 4-5 m/s, such as in the north-west Pacific and Atlantic ocean (between 20°N and 30°N) and in the south-east Pacific and Atlantic ocean (between 20°S and 30°S), the ECMWF C_D is similar or slightly smaller than NCAR.

Since the wind stress is not affected by the type of first-order feedback at play for the NSHFs (SST-Q_T negative feedback, see Section 2.2), differences in U and C_D between experiments are reflected in the resulting different fields after bulk calculation (i.e. τ and WSC, Figure 10). Over the ACC, the northern and southern mid-latitudes (e.g. EBUS), and the Atlantic storm track (i.e. regions characterized by wind speeds above $5m/s$ and ECMWF_NS C_D larger than CdNC_CeEC_NS C_D, see Figure 10), the ECMWF_NS wind stress is stronger by an average of $0.035N/m^2$ (about 20% of NCAR absolute value) with respect to NCAR. In the 5°N - 10°N region, which is a latitudinal band characterized by mean winds below $5m/s$ and C_D larger in CdNC_CeEC_NS than ECMWF_NS (Figure 10), ECMWF_NS shows a wind stress reduction of -$0.003N/m^2$ (about 3% of NCAR absolute value) with respect to NCAR. In regions where the differences in C_D and wind stress are opposite (e.g. the north-west and south-west Pacific and Atlantic ocean, Indian ocean, Baja California, Equatorial warm pool), the inclusion of convective gustiness in the U calculation may play a role in strengthening the wind stress in ECMWF_NS (9a). In addition,

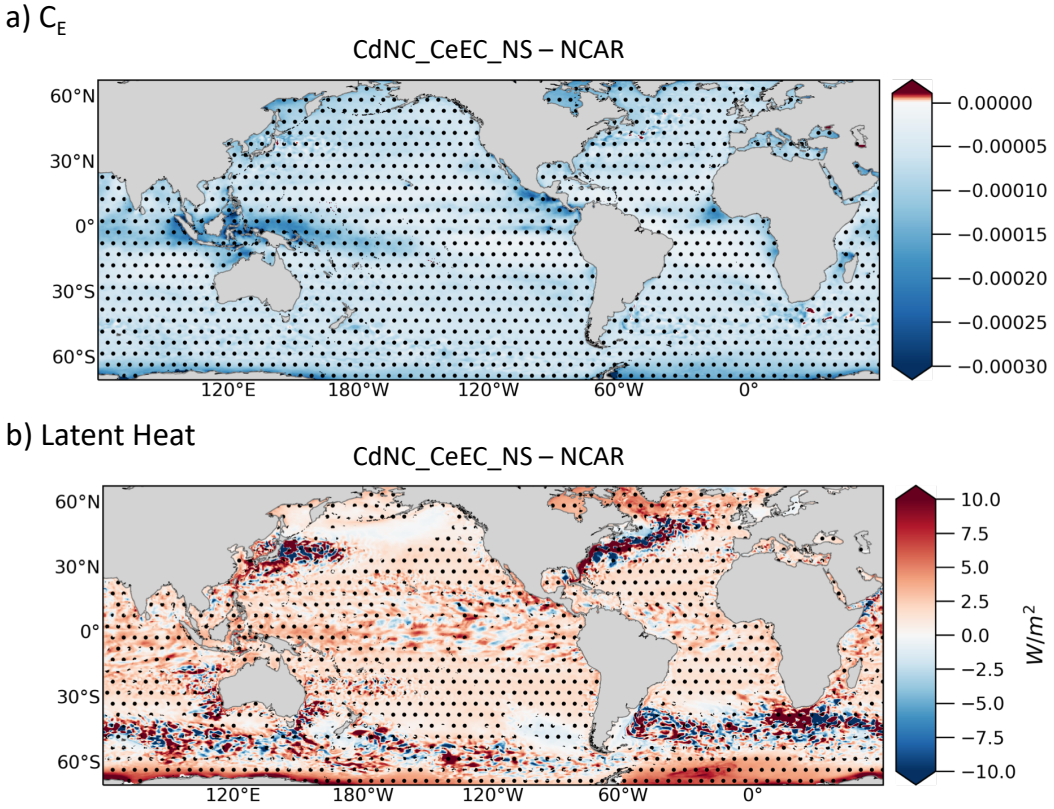

Figure 8. Annual mean differences of a) specific humidity transfer coefficient (C_E), b) latent heat between CdNC_CeEC_NS and NCAR

the high time-variability of the C_D differences (not shown) could hide the relation between C_D and τ. Both hypotheses are verified, the ECMWF_NS experiment presents a stronger wind stress almost everywhere over the global ocean compared to a twin experiment (i.e. ECMWF_NS_NG) where the convective gustiness is not used in the computation (Figure S4) and the correlation between C_D differences and wind stress differences is always significant and positive (not shown). The higher the difference in C_D, the stronger the differences in wind stress.

The SST differences between ECMWF_NS and CdNC_CeEC_NS over the tropical Pacific and Atlantic Oceans (Figure 6b) are probably related to Ekman suction, which is driven by the positive (negative) wind stress curl in the northern (southern) hemisphere. Substantial differences were found in ECMWF_NS compared to CdNC_CeEC_NS, characterized by greater mean wind stress both north and south of the tropical band and weaker wind stress along the equator (Figure 10a). These latitudinal differences in wind stress between experiments are reflected in the differences in the wind stress curl patterns (Figure 10b). Indeed, a stronger acceleration (deceleration) of southeast trades north (south) of the equator in ECMWF_NS may lead to a stronger positive (negative) curl north (south) of the Equator. This relation was found to be significant north of the equator: the stronger positive wind stress curl in ECMWF_NS than CdNC_CeEC_NS resulted in a colder SST in ECMWF_NS compared to

CdNC_CeEC_NS (see correlation map in Figure S5).

The stronger wind stress along EBUS in ECMWF_NS compared to CdNC_CeEC_NS, instead, probably enhances coastal upwelling, explaining most of the SST differences over these regions. Part of the SST difference could also be related to Ekman suction. ECMWF_NS shows stronger positive (negative) wind stress curl in the northern (southern) hemisphere EBUS compared to CdNC_CeEC_NS (Figure 10b). The vertical velocity, and in turn, the coastal SST along EBUS are, indeed, extremely sensitive to wind forcing changes (Bonino et al., 2019; Small et al., 2015; Capet et al., 2004; Desbiolles et al., 2014). These relations were confirmed along the coast of the Benguela Upwelling System (Figures S6 and S6). During the Benguela upwelling season (ONDJ), the enhanced wind stress and negative wind stress curl in ECMWF_NS reinforce the vertical velocity with respect to CdNC_CeEC_NS (Figure S6), resulting in a colder surface temperature (see correlation maps Figure S7).

The differences in the wind stress are also responsible for the changes in the meridional heat transport. MHT differences between ECMWF_NS and CdNC_CeEC_NS resemble the differences between ECMWF_S and NCAR (compare Figure 4c and Figure 11c), with higher transport in ECMWF_NS at all latitudes. The largest differences are located in the tropical region (up to 0.6 PW, about 18% of NCAR mean value), where the differences in meridional transport (linked to the equatorial upwelling) between the two experiments are likely maxima.

Although the two experiments use the same C_E and C_H, the dependence of Q_L and Q_H on the prognostic SST at each time-step generates differences in Q_T (Figure 11a). The ocean gains heat in ECMWF_NS compared to CdNC_CeEC_NS (i.e. positive Q_T differences) over the EBUS and the Equatorial region. In contrast to the previous finding, the differences in Q_T and SST have an opposite sign, indicating that SST differences drive the Q_T differences: the colder the temperature produced by ECMWF_NS wind stress with respect to CdNC_CeEC_NS, the higher the heat gained by ECMWF_NS along the latitudes (Figure 11b). In summary, ECMWF_NS reproduces stronger wind stress and wind stress curl along EBUS, and stronger cyclonic wind stress curl along the Equator, which generate colder SST with respect to CdNC_CeEC_NS, through enhanced upwelling processes.

Given the importance of wind stress in driving the SST differences between ECMWF and NCAR parameterizations, we now examine why COARE_S does not show the cold SST differences in comparison to NCAR over EBUS and the equatorial Pacific (Figure 4b). With wind speeds ranging from 7 to 9 m/s (e.g. over EBUS), the C_D in the COARE_S parameterization is smaller than that of the ECMWF parameterization, but slightly higher or almost identical (around 7 m/s) than the C_D of NCAR (refer to Figure 1c). Moreover, over the northern equatorial band, the C_D of COARE_S is smaller than that of ECMWF_S and NCAR. As a consequence, the COARE_S differences in wind stress (Figure 3a) in comparison with NCAR are characterized by a strong decrease, roughly 10%, over the northern equatorial band and a slight increase in the wind stress, roughly 2%, over EBUS. The increase in wind stress over EBUS in COARE_S (2% in comparison to 25% in ECMWF_S) is insufficient to promote stronger coastal upwelling in the annual mean, and in turn colder SST with respect to NCAR. As regards the equatorial upwelling, the weak increase in the wind stress in the northern equatorial region (e.g. northern equatorial cold front) compared to NCAR wind stress (Figure 3a), prevents the enhancement of the positive wind stress curl in COARE_S (Figure 3c). However, to properly identify the drivers of the pattern in SST differences between COARE_S and NCAR , further numerical experiments need to be performed.

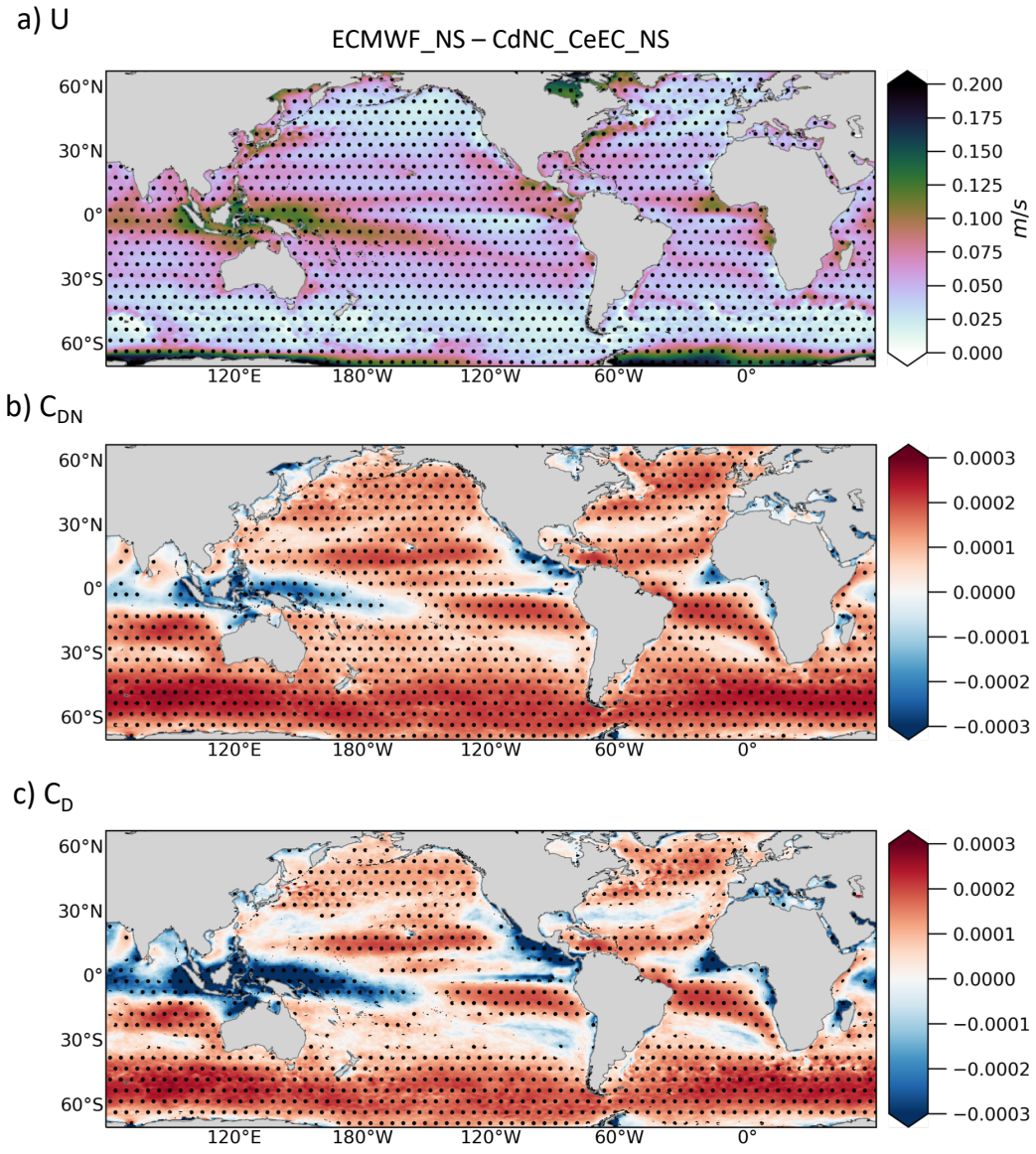

Figure 9. Annual mean differences in a) wind speed (U), b) neutral wind stress transfer coefficient (C_{DN}) and c) wind stress transfer coefficient (C_D) between `ECMWF_NS` and `CdNC_CeEC_NS`. Hatching indicates significant values (95% confidence level).

3.5 Online prognostic SST approach vs offline prescribed SST approach

In order to discuss the role of the SST-Q_T negative feedback at play in the online prognostic SST approach, we compared our results with Brodeau et al. (2017), who compared the different bulk parameterizations using the offline prescribed SST approach (i.e. TASFs are computed by means of bulk formulas using prescribed surface atmospheric variables and prescribed

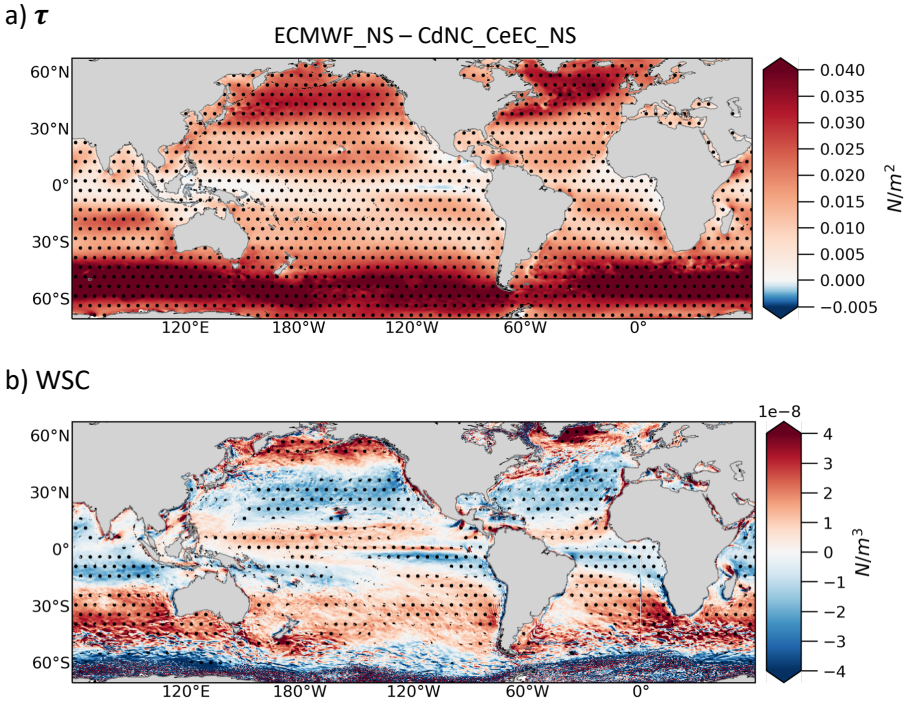

Figure 10. Annual mean differences in a) wind stress (τ) and b) wind stress curl (WSC) between ECMWF_NS and CdNC_CeEC_NS.

SST). There are a few discrepancies in the bulk implementation between this study and Brodeau et al. (2017). The latter authors used the COARE3.0 parameterization instead of COARE3.6 and, their simulations, which were performed for a longer (1982-2014) period, were forced by the ERA-Interim reanalysis instead of ERA5. Our aim in this comparison is therefore only to qualitatively understand the negative feedback between the SST and the Q_T at play in our experiments.

Brodeau et al. (2017) report a mean global increase in the wind stress of $20mN/m^2$ using ECMWF parameterization instead of NCAR parameterization. The computation of the wind stress is not affected by the SST-Q_T negative feedback (see equation 1a). This means that our result of the $20mN/m^2$ global mean increase in wind stress is completely in line with the prescribed SST comparison by Brodeau et al. (2017). Our findings do not follow Brodeau et al. (2017) in terms of the Q_T differences between ECMWF_S and NCAR parameterizations. The latter authors found a global mean increase in Q_T of $13W/m^2$ for ECMWF_S, while in our experiments ECMWF_S showed a mean global increase of $5W/m^2$ with respect to NCAR. Moreover, they report an increase of $7W/m^2$ considering SSTskin rather than SST in the COARE parameterization, while in our experiments ECMWF_S showed a mean global increase of $1W/m^2$ with respect to ECMWF_NS. The negative feedback between the SST and the Q_T which is active in our experiments reduced the differences in the total turbulent flux across parameterizations compared to the prescribed SST comparison.

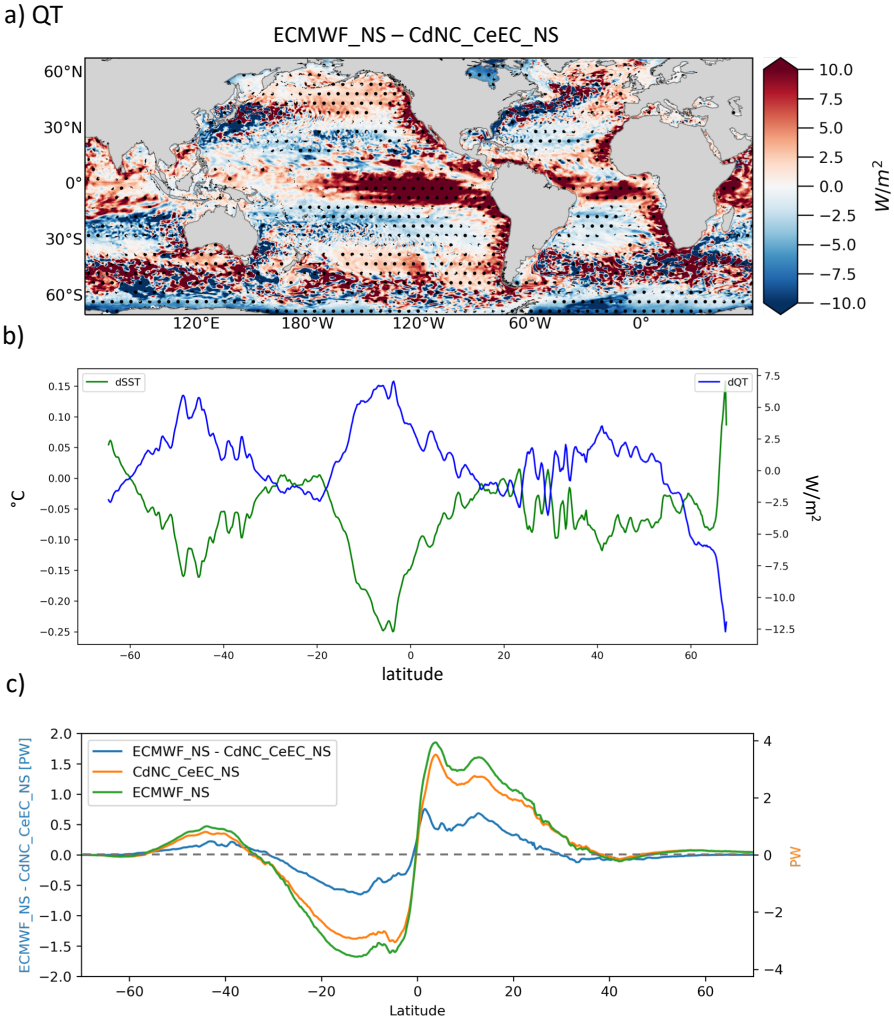

Figure 11. a) Annual mean differences in turbulent heat fluxes (Q_T) between `ECMWF_NS - CdNC_CeEC_NS`; b) Annual zonal-mean differences time-series of SST (green) and Q_T (blue) between `ECMWF_NS - CdNC_CeEC_NS`; c) Global Meridional Heat Transport in the upper 100m ocean (values on the right y axis) for `ECMWF_NS` and `CdNC_CeEC_NS` and differences (values on the left y axis) between them. Hatching indicates significant values (95% confidence level).

4 Summary and conclusions

In this work we have investigated how the implementation of different bulk parameterizations in the NEMOv4 ocean general circulation model drives substantial changes in prognostic sea surface temperature. Specifically, we studied the contribution of different aspects and assumptions of the bulk parameterizations in driving the SST differences across numerical experiments performed using the NEMO global model configuration with 1/4° of horizontal resolution. We analyzed and quantified the

role of the inclusion of the skin temperature in the computation of the turbulent heat flux components, and we also studied the role of the turbulent heat flux components and of the wind stress in driving the SST changes between parameterizations. We analysed annual mean TASF differences between 'control experiments', short-term numerical experiments which used the bulk parameterizations implemented in NEMOv4, and 'mixed experiments', short-term sensitivity experiments where bulk assumptions are excluded (e.g. skin temperature) or bulk transfer coefficients are computed mixing the bulk parameterizations (e.g. C_D from NCAR parameterization and C_E and C_H from ECMWF parameterization). In addition to highlighting the sensitivity of the sea surface temperature to the bulk parameterizations, we believe that the importance of this work is also the examination of the role of the SST-Q_T negative feedback in the simulations. We compared the modeled turbulent air-sea fluxes with the estimations by Brodeau et al. (2017), who analyzed the same bulk parameterizations, but using the offline prescribed SST approach. Our findings can be summarized as follow:

1. The implementation of skin temperature in the bulk parameterizations reduces evaporation and decreases the turbulent heat flux to the atmosphere, thus promoting ocean warming. The skin temperature is usually colder than the sea surface temperature. The skin temperature contribution in terms of turbulent heat flux is weaker than the Brodeau et al. (2017) estimations due to the negative feedback between the SST and the Q_T. In our experiments SST is free to evolve and feeds back negatively with respect to Q_T.

2. The turbulent heat flux differences between experiments are dominated by the latent heat flux, which arises from C_E differences between bulk parameterizations. Less evaporative ocean gains heat, which tends to promote ocean warming. The turbulent heat flux differences are weaker than the estimations of Brodeau et al. (2017) and can be attributed to the SST-Q_T negative feedback.

3. The wind stress differences between bulk parameterizations are attributable to the C_D differences, especially in wind-driven dominantly ocean regions. Experiments with enhanced wind stress or wind stress curl over EBUS and over Equatorial Pacific promote upwelling processes and consequent cooling of the sea surface temperature. Stronger wind stress causes an increase in the poleward heat transport in the upper ocean, which leads to a more pronounced increase in the $\neg\pm$20°N latitude band. The wind stress differences across the bulk parameterizations implemented in NEMOv4 are of the same magnitude as the wind stress differences calculated by Brodeau et al. (2017). This is due to the fact that, at first order, the wind stress computation is not affected by the SST.

We used forced ocean experiments in which the atmospheric fields (e.g. wind, air temperature, air humidity) to the ocean model and seen in the online prognostic SST approach come from an atmospheric reanalysis, and do not respond back to the ocean variability. Introducing the air-sea feedback in the system might substantially impact on the turbulent fluxes and modify our findings in terms of comparing the SST response among the bulk parameterizations. In order to improve the representation of air-sea interaction in the NEMO framework, an atmospheric boundary layer (ABL) has been integrated in the new NEMO release 4.2 (Lemarié et al., 2021). However, the ABL implementation is in a preliminary stage and the current online prognostic SST approach is still the most commonly used. Although the new release of NEMO, v4.2, includes some modifications to the bulk formula version used in this study, these changes do not affect the results presented in this paper.

Appendix A: Table A1

List of Acronyms and Symbols

Acronym	Expansion
TASFs	Turbulent Air-Sea Flux components
THFs	Turbulent Heat Flux components
NSHFs	Non Solar Heat Flux components
Q_T	Total turbulent heat flux
BTC	Bulk Transfer Coefficient
SSTSkin	Sea Surface Skin Temperature
CSWL	Cool Skin and (diurnal) Warm Layer
EBUS	Eastern Boundary Upwelling Systems
MHT	Meridional Heat Transport
WSC	Wind Stress Curl

Code availability. This version of the NEMO code is based on code release 4.0, revision number 12957 (https://forge.ipsl.jussieu.fr/nemo/browser/NEMO/trunk?rev=12957, last access: 24 February 2022). All the codes to estimate TASFs in the NEMOv4.0 framework, originates from this AeroBulk package, which is completely open source and available at https://github.com/brodeau/aerobulk (Brodeau et al., 2017). The original code was modified in the computations of the bulk transfer coefficients applied to perform the experiments. The code and the namelists to run each experiment are available in the Zenodo archive (https://doi.org/10.5281/zenodo.6258085, DOI: 10.5281/zenodo.6258085). The model outputs used to produce the figures are also available in the Zenodo archive.

Author contributions. GB modified the numerical code, set up the experiment and wrote the manuscript. DI conceived and designed this study. All authors contributed to the interpretation of results and editing.

Competing interests. The authors declare that they have no conflict of interest.

Acknowledgements. We gratefully acknowledge support through EU project IMMERSE (H2020 Grant Agreement N. 821926). We also acknowledge the CMCC Foundation for having provided computational resources.

References

Amante, C. and Eakins, B. W.: ETOPO1 arc-minute global relief model: procedures, data sources and analysis, 2009.

Barnier, B.: Forcing the ocean, in: Ocean modeling and parameterization, pp. 45–80, Springer, 1998.

Bernard, B., Madec, G., Penduff, T., Molines, J.-M., Treguier, A.-M., Le Sommer, J., Beckmann, A., Biastoch, A., Böning, C., Dengg, J., et al.: Impact of partial steps and momentum advection schemes in a global ocean circulation model at eddy-permitting resolution, Ocean dynamics, 56, 543–567, 2006.

Blanke, B. and Delecluse, P.: Variability of the tropical Atlantic Ocean simulated by a general circulation model with two different mixed-layer physics, Journal of Physical Oceanography, 23, 1363–1388, 1993.

Bonino, G., Masina, S., Iovino, D., Storto, A., and Tsujino, H.: Eastern Boundary Upwelling Systems response to different atmospheric forcing in a global eddy-permitting ocean model, Journal of Marine Systems, 197, 103 178, 2019.

Bonino, G., Iovino, D., and Masina, S.: Bulk Formulations in NEMOv.4:algorithms review and sea surface temperature response in ORCA025case study, Technical Notes No. 289, https://doi.org/10.25424/cmcc/bulk_formulas_nemo_report, 2020.

Bradley, E. and Fairall, C.: A guide to making climate quality meteorological and flux measurements at sea, 2007.

Brodeau, L., Barnier, B., Gulev, S. K., and Woods, C.: Climatologically significant effects of some approximations in the bulk parameterizations of turbulent air–sea fluxes, Journal of Physical Oceanography, 47, 5–28, 2017.

Capet, X., Marchesiello, P., and McWilliams, J.: Upwelling response to coastal wind profiles, Geophysical Research Letters, 31, 2004.

Chen, D., Busalacchi, A. J., and Rothstein, L. M.: The roles of vertical mixing, solar radiation, and wind stress in a model simulation of the sea surface temperature seasonal cycle in the tropical Pacific Ocean, Journal of Geophysical Research: Oceans, 99, 20 345–20 359, 1994.

Dai, A. and Trenberth, K. E.: Estimates of freshwater discharge from continents: Latitudinal and seasonal variations, Journal of hydrometeorology, 3, 660–687, 2002.

Dai, A., Qian, T., Trenberth, K. E., and Milliman, J. D.: Changes in continental freshwater discharge from 1948 to 2004, Journal of climate, 22, 2773–2792, 2009.

de Szoeke, S. P., Marke, T., and Brewer, W. A.: Diurnal ocean surface warming drives convective turbulence and clouds in the atmosphere, Geophysical Research Letters, 48, e2020GL091 299, 2021.

Desbiolles, F., Blanke, B., Bentamy, A., and Grima, N.: Origin of fine-scale wind stress curl structures in the Benguela and Canary upwelling systems, Journal of Geophysical Research: Oceans, 119, 7931–7948, 2014.

Desbiolles, F., Alberti, M., Hamouda, M. E., Meroni, A. N., and Pasquero, C.: Links between sea surface temperature structures, clouds and rainfall: Study case of the Mediterranean Sea, Geophysical Research Letters, 48, e2020GL091 839, 2021.

Edson, J. B., Jampana, V., Weller, R. A., Bigorre, S. P., Plueddemann, A. J., Fairall, C. W., Miller, S. D., Mahrt, L., Vickers, D., and Hersbach, H.: On the exchange of momentum over the open ocean, Journal of Physical Oceanography, 43, 1589–1610, 2013.

Fairall, C. W., Bradley, E. F., Rogers, D. P., Edson, J. B., and Young, G. S.: Bulk parameterization of air-sea fluxes for tropical ocean-global atmosphere coupled-ocean atmosphere response experiment, Journal of Geophysical Research: Oceans, 101, 3747–3764, 1996.

Fairall, C. W., Bradley, E. F., Hare, J., Grachev, A. A., and Edson, J. B.: Bulk parameterization of air–sea fluxes: Updates and verification for the COARE algorithm, Journal of climate, 16, 571–591, 2003.

Gaube, P., Chickadel, C., Branch, R., and Jessup, A.: Satellite observations of SST-induced wind speed perturbation at the oceanic submesoscale, Geophysical Research Letters, 46, 2690–2695, 2019.

Gill, A. E.: Atmosphere-ocean dynamics, Int. Geophys. Ser., 30, 662p, 1982.

Hersbach, H., Bell, B., Berrisford, P., Hirahara, S., Horányi, A., Muñoz-Sabater, J., Nicolas, J., Peubey, C., Radu, R., Schepers, D., et al.: The ERA5 global reanalysis, Quarterly Journal of the Royal Meteorological Society, 146, 1999–2049, 2020.

IOC, I.: BODC. Centenary edition of the gebco digital atlas, Digital Media, 2003.

Jacobs, S. S., Hellmer, H. H., and Jenkins, A.: Antarctic ice sheet melting in the Southeast Pacific, Geophysical Research Letters, 23, 957–960, 1996.

Kara, A. B., Rochford, P. A., and Hurlburt, H. E.: Efficient and accurate bulk parameterizations of air–sea fluxes for use in general circulation models, Journal of Atmospheric and Oceanic Technology, 17, 1421–1438, 2000.

Large, W. and Pond, S.: Open ocean momentum flux measurements in moderate to strong winds, Journal of physical oceanography, 11, 324–336, 1981.

Large, W. and Pond, S.: Sensible and latent heat flux measurements over the ocean, Journal of physical Oceanography, 12, 464–482, 1982.

Large, W. and Yeager, S.: The global climatology of an interannually varying air–sea flux data set, Climate dynamics, 33, 341–364, 2009.

Lemarié, F., Samson, G., Redelsperger, J.-L., Giordani, H., Brivoal, T., and Madec, G.: A simplified atmospheric boundary layer model for an improved representation of air–sea interactions in eddying oceanic models: implementation and first evaluation in NEMO (4.0), Geoscientific Model Development, 14, 543–572, 2021.

Levitus, S., Antonov, J., Baranova, O., Boyer, T., Coleman, C., Garcia, H., Grodsky, A., Locarnini, R., Mishonov, A., Reagan, J., et al.: The world ocean database, Data Science Journal, 12, WDS229–WDS234, 2013.

Li, Y. and Carbone, R.: Excitation of rainfall over the tropical western Pacific, Journal of the atmospheric sciences, 69, 2983–2994, 2012.

Madec, G. and Imbard, M.: A global ocean mesh to overcome the North Pole singularity, Climate Dynamics, 12, 381–388, 1996.

Madec G. and NEMO System Team: NEMO ocean engine, Scientific Notes of Climate Modelling Center, 27 — ISSN 1288-1619, Institut Pierre-Simon Laplace (IPSL), https://doi.org/10.5281/zenodo.1464816.

Merchant, C. J., Embury, O., Bulgin, C. E., Block, T., Corlett, G. K., Fiedler, E., Good, S. A., Mittaz, J., Rayner, N. A., Berry, D., et al.: Satellite-based time-series of sea-surface temperature since 1981 for climate applications, Scientific data, 6, 1–18, 2019.

Monin, A. S. and Obukhov, A. M.: Basic laws of turbulent mixing in the surface layer of the atmosphere, Contrib. Geophys. Inst. Acad. Sci. USSR, 151, e187, 1954.

NEMO Sea Ice Working Group: Sea Ice modelling Integrated Initiative (SI^3) – The NEMO sea ice engine, 2020.

Renault, L., Lemarié, F., and Arsouze, T.: On the implementation and consequences of the oceanic currents feedback in ocean–atmosphere coupled models, Ocean Modelling, 141, 101 423, 2019a.

Renault, L., Masson, S., Oerder, V., Jullien, S., and Colas, F.: Disentangling the mesoscale ocean-atmosphere interactions, Journal of Geophysical Research: Oceans, 124, 2164–2178, 2019b.

Renault, L., Masson, S., Arsouze, T., Madec, G., and Mcwilliams, J. C.: Recipes for how to force oceanic model dynamics, Journal of Advances in Modeling Earth Systems, 12, e2019MS001 715, 2020.

Seager, R., Blumenthal, M. B., and Kushnir, Y.: An advective atmospheric mixed layer model for ocean modeling purposes: Global simulation of surface heat fluxes, Journal of climate, 8, 1951–1964, 1995.

Shriver, J. F. and Hurlburt, H. E.: The contribution of the global thermohaline circulation to the Pacific to Indian Ocean throughflow via Indonesia, Journal of Geophysical Research: Oceans, 102, 5491–5511, 1997.

Siedler, G., Griffies, S. M., Gould, J., and Church, J. A.: Ocean circulation and climate: a 21st century perspective, Academic Press, 2013.

Small, R. d., deSzoeke, S. P., Xie, S., O'neill, L., Seo, H., Song, Q., Cornillon, P., Spall, M., and Minobe, S.: Air–sea interaction over ocean fronts and eddies, Dynamics of Atmospheres and Oceans, 45, 274–319, 2008.

Small, R. J., Curchitser, E., Hedstrom, K., Kauffman, B., and Large, W. G.: The Benguela upwelling system: Quantifying the sensitivity to resolution and coastal wind representation in a global climate model, Journal of Climate, 28, 9409–9432, 2015.

Smith, S. D.: Coefficients for sea surface wind stress, heat flux, and wind profiles as a function of wind speed and temperature, Journal of Geophysical Research: Oceans, 93, 15 467–15 472, 1988.

Sun, Z., Liu, H., Lin, P., Tseng, Y.-h., Small, J., and Bryan, F.: The modeling of the North Equatorial Countercurrent in the Community Earth System Model and its oceanic component, Journal of Advances in Modeling Earth Systems, 11, 531–544, 2019.

Swenson, M. S. and Hansen, D. V.: Tropical Pacific Ocean mixed layer heat budget: The Pacific cold tongue, Journal of Physical Oceanography, 29, 69–81, 1999.

Torres, O., Braconnot, P., Marti, O., and Gential, L.: Impact of air-sea drag coefficient for latent heat flux on large scale climate in coupled and atmosphere stand-alone simulations, Climate Dynamics, 52, 2125–2144, 2019.

Yuen, C., Cherniawsky, J., Lin, C., and Mysak, L.: An upper ocean general circulation model for climate studies: Global simulation with seasonal cycle, Climate dynamics, 7, 1–18, 1992.

Zalesak, S. T.: Fully multidimensional flux-corrected transport algorithms for fluids, Journal of computational physics, 31, 335–362, 1979.